THE JOURNAL OF PHYSICAL CHEMISTRY B

pubs.acs.org/JPCB Article

Vibronic Quantum Beating between Electronic Excited States in a Heterodimer

Published as part of The Journal of Physical Chemistry virtual special issue "Peter J. Rossky Festschrift".

V. M. Freixas, S. Tretiak, D. V. Makhov, D. V. Shalashilin, and S. Fernandez-Alberti*

Cite This: *J. Phys. Chem. B* 2020, 124, 3992–4001 Read Online

ABSTRACT: Energy transfer in multichromophoric molecules can be affected by coherences that are induced by the electronic and vibrational couplings between chromophore units. Coherent electron-vibrational dynamics can persist at the subpicosecond time scale even at room temperature. Furthermore, wave-like localized-delocalized motions of the electronic wave function can be modulated by vibrations that actively participate in the intermolecular energy transfer process. Herein, nonadiabatic excited state molecular dynamics simulations have been performed on a rigid synthetic heterodimer that has been proposed as a simplified model for investigating the role and mechanism of coherent energy transfer in multichromophoric systems. Both surface hopping (SH) and Ehrenfest approaches (EHR) have been considered. After photoexcitation of the system at room temperature, EHR simulations reveal an ultrafast beating of electronic populations between the two lowest electronic states. These oscillations are not observed at low temperature and have vibrational origins. Furthermore, they cannot be reproduced using SH approach. This periodic behavior of electronic populations induces oscillations in the spatial localization of the electronic transition density between monomers. Vibrations whose frequencies are near-resonant with energy difference between the two lowest electronic excited states are in the range of the electronic population beating, and they are the ones that contribute the most to the coherent dynamics of these electronic transitions.

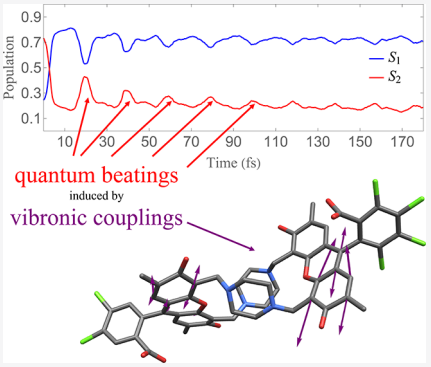

I. INTRODUCTION

Efficient solar light harvesting underpins many clean renewable energy technologies. However, achieved state of the art is still subpar to natural photosynthetic examples. Multiple studies (for example, refs 1−7) suggested that oscillatory quantum dynamics may play a role in the energy funneling of light harvesting antennas present in living organisms. It has been hypothesized that quantum coherence can contribute to intermolecular energy transfer efficiency by minimizing its dissipation to the environment.[4,6,8−10] This scenario was also proposed for large multichromophoric molecules at room temperature.[1,11−14] Therefore, it becomes necessary to clarify if long-lived coherent dynamics may represent an additional feature to take into account for the design of artificial light harvesting devices mimicking natural systems. To this end, neither the numerous experimental studies[3,15,16] nor the theoretical models[17−27] were able to achieve a complete description of the atomistic origins of the observed quantum beatings.

Persistent quantum coherence, discovered in natural[4] and artificial[8,28−31] multichromophoric light harvesting systems was originally attributed to solely electronic degrees of freedom, and later has been associated with the complex interactions between vibrational and electronic (vibronic) degrees of freedom during coherent exciton−vibrational dynamics.[32,33]

A common scenario for energy transfer in multichromophores involves nonadiabatic (i.e., beyond Born−Oppenheimer approximation) evolution of electronic populations involving multiple electronic states.[8,33] Nowadays, strong evidence support the idea that coherent exciton−vibrational dynamics, that emerge from nonadiabatic transitions between excited states, can persists over long (frequently picosecond) time scales at room temperature.[4−7] Nonadiabatic transitions between excited states funnel the energy transfer through specific classical vibrational motions that modulate the wave-like localized−delocalized motion of the electronic wave function.[34] That is, the nonequilibrium dynamics of such selected vibrations can be manifested itself in ultrafast beating of excitonic populations.[25,26,35−40]

The photoexcitation and subsequent electronic and vibrational energy redistribution and relaxation in multichromophoric molecular systems involve processes like internal

Received: February 26, 2020
Revised: April 17, 2020
Published: April 20, 2020

https://dx.doi.org/10.1021/acs.jpcb.0c01685
J. Phys. Chem. B 2020, 124, 3992−4001

conversion, and transient exciton localization/delocalization, and couplings among the multiple electronic and vibrational excited states that actively participate in the process. In order to achieve an atomistic description of such processes, molecular dynamics simulations involving several coupled electronic excited states and vibrational degrees of freedom are required.

Ab initio quantum direct dynamics[41,42] (QDD) simulations of light harvesting apparatus in living organisms are still too expensive computationally to study detailed photoinduced dynamics in multichromophoric molecular systems involving a large number of coupled electronic excited states.[43−46] Hybrid quantum/classical methods are presently less computationally expensive alternatives to deal with nonadiabatic excited states molecular dynamics simulations.[41,47] Within this context, surface hopping[48−51] (SH) and Ehrenfest approaches are among the less computationally expensive and therefore extensively used to study a wide variety of organic molecules.[52−59] The multi-configurational Ehrenfest approach[44] (MCE) is a generalization of EHR in which several independent Ehrenfest trajectories are used to guide as a basis set to represent the full quantum wave function of electrons and nuclei. In the existing implementations, quantum coupling between the trajectory guided basis functions is calculated afterward as a postprocessing, allowing a highly parallelizable implementation. Several sampling techniques[60] have been developed to cover relevant regions of the configuration space, making the MCE flexible to study a wide range of molecular systems. In particular, the ab initio multiple cloning[61,62] (AIMC) extension plays the role of recovering the right physical meaning of the Ehrenfest mean field allowing the nuclear wave function to bifurcate in configuration space, increasing the basis size whenever it is needed. Furthermore, the time-dependent diabatic basis[63] (TDDB) implementation allows excited states to swap at trivial unavoided crossings.[64] Our recent AIMC implementation in the TDDB combines the MCE algorithms with the on-the-fly calculation of excited states energies, gradients, and nonadiabatic couplings within the non-adiabatic excited state molecular dynamics (NEXMD) package.[65−69]

In the present work, NEXMD simulations[47] have been performed on a rigid synthetic heterodimer that has been proposed as a simplified model for investigating the role and mechanism of coherent energy transfer in multichromophoric systems.[19,29] The presence of long-lived coherences has been evidenced as quantum beating signals in two-dimensional (2D) electronic spectroscopy.[29] These oscillations were modeled computationally[19] by combining adiabatic molecular dynamics simulations with electronic structure calculations, and this study focused on the identification of the inverse relationship between decoherence times and the magnitude of the energy gap fluctuation. Nevertheless, the role of nonadiabatic couplings on excited-state gradients guiding the excess of energy flux through specific vibrational modes and assisting quantum coherence has yet to be explored.

Here, in order to analyze the origin of these quantum beatings, simulations using AIMC-MCE, EHR, and SH approaches have been performed. It is often believed that, for modeling of nonadiabatic dynamics, EHR method usually works worse than SH. In this paper we are making Ehrenfest approach great again. We show that for this particular system that EHR result is almost indistinguishable from that of more rigorous, but at the same time complicated, AIMC-MCE approach. After photoexcitation of the system at room temperature, EHR simulations reveal an ultrafast beating of S_1 and S_2 electronic populations. We found that these oscillations are induced by specific active vibrational normal modes coupled to electronic system in the direction of the nonadiabatic energy transfer between excited states. However, SH dynamics is qualitatively different from that of EHR and fully quantum AIMC-MCE in the sense that SH cannot reproduce the beatings.

The paper is organized as follows: In section II we present our working equations and numerical details regarding the preparation of the initial conditions. We discuss results in section III, and finally in section IV we make our concluding remarks.

II. METHODS

II.A. Ehrenfest (EHR) and Surface Hopping (SH) Simulations within the NEXMD Framework. Within EHR and SH[48−51] approaches, the electronic degrees of freedom are propagated quantum mechanically, while the motions of the nuclei are treated classically. In EHR simulations nuclei evolve on a mean field potential energy surface (PES) having a weighted contribution from all electronic excited states, and the force F driving them is given by

$$\mathbf{F} = -\sum_I |a_I|^2 \nabla_{\mathbf{R}} E_I + \sum_{I,J} (a_I)^* a_J \mathbf{d}_{IJ} (E_I - E_J) \tag{1}$$

where the electronic wave function $|\psi\rangle$ is expanded on the basis of adiabatic electronic states $|\psi\rangle = \Sigma_I a_I|\phi_I\rangle$, E_I is the Ith PES, $\nabla_{\mathbf{R}}$ is the gradient respect to the nuclear coordinates R, and d_{IJ} are the nonadiabatic derivative coupling vectors ($NACR_{IJ}$) between adiabatic electronic state I and J:

$$\mathbf{d}_{IJ} = \langle \phi_I | \nabla_{\mathbf{R}} | \phi_J \rangle \tag{2}$$

In SH, nuclei evolve on a PES that is defined by a single electronic state at a given time and transitions (hops) from one electronic state to another are dictated by the evolution in time of the coefficients of the electronic wave function. For all methods in this work, these are propagated as

$$\dot{a}_I = -\frac{i}{\hbar} E_I a_I - \sum_J \dot{\mathbf{R}} \cdot \mathbf{d}_{IJ} a_J \tag{3}$$

with $\dot{R}\cdot d_{IJ}$ being the nonadiabatic coupling terms ($NACT_{IJ}$) and $\dot{R}$ the nuclei velocity vector.

Both EHR and SH have been implemented within the NEXMD[47,70] framework that has been specifically developed to model photoinduced dynamics in large conjugated molecules involving multiple coupled electronically excited states. It combines either EHR or SH methods with "'on the fly'" analytical calculations of excited-state energies,[69,71,72] gradients,[73,74] and nonadiabatic coupling terms.[47,75−77] The collective electronic oscillator (CEO) approach[66−68] is used at the configuration interaction singles (CIS) level with the semiempirical AM1 Hamiltonian.[78]

The NEXMD framework, either in its EHR and SH implementation (i.e., EHR-NEXMD and SH-NEXMD), has been proved to be accurate enough to achieve a qualitative description of the photoinduced intramolecular energy in a large variety of multichromophoric molecular systems.[33,62,63,79,80] More details about the NEXMD approach,

https://dx.doi.org/10.1021/acs.jpcb.0c01685
J. Phys. Chem. B 2020, 124, 3992−4001

implementation, advantages and testing parameters can be found elsewhere.[47,70,81]

NEXMD simulations allow us to analyze spatial exciton localization by calculating transition density matrices (TDM)[82,83] $(\rho_I^{(n)})_{i,j} = \langle \phi_I^{(n)} | c_i^\dagger c_j | \phi_g^{(n)} \rangle$. $c_i^\dagger$ and c_j are the electron creation and annihilation operators applied over atomic orbitals (AO) i and j, and $|\phi_g^{(n)}\rangle$ represents the ground state wave function. In multichromophoric molecular system, the spatial exciton localization can be evaluated as the fraction of electronic transition density localized on each chromophore unit by summing up $(\rho_I^{(n)})_{i,j}$ over all AO corresponding to atoms localized in each unit. More details about TDM analysis, either using EHR, SH, and MCE approaches can be found elsewhere.[61,62,84]

II.B. Multiconfigurational Ehrenfest (MCE) and ab Initio Multiple Cloning (AIMC) Methods. MCE is a natural generalization of EHR dynamics in which we describe our molecule by means of a wave function $|\Psi(t)\rangle$ which is given by a linear combination of configurations $|\psi_n\rangle$. Each configuration consists of a nuclear part $|\chi_n\rangle$ and an electronic part. The nuclear part is given by coherent states,[60,85] which in the coordinate representation are Gaussian functions centered in EHR trajectories with coordinates R_n and momenta P_n. The electronic part is given by a linear combination of adiabatic excited states $|\phi_I^{(n)}\rangle$:

$$|\Psi(t)\rangle = \sum_n c_n |\psi_n\rangle = \sum_n c_n |\chi_n\rangle \sum_I a_I^{(n)} |\phi_I^{(n)}\rangle \tag{4}$$

Here, the superindex n denotes the n^{th} configuration. In principle, the wave function (4) can be converged to the exact result, but in practice it is a difficult task especially for a Direct Dynamics method.

The main computational strength of this method is that EHR trajectories can be simulated in parallel, and the configuration amplitudes c_n can be calculated afterward.[44] More details about MCE and its implementation within the NEXMD framework can be seen elsewhere.[44,63]

Since the MCE makes use of the EHR trajectory-guided basis functions, different sampling techniques have been proposed to ensure that EHR trajectories span through all relevant regions of configuration space.[60] The ab initio multiple cloning (AIMC)[61,86] method has been developed to overcome situations in which the excess energy flow can follow different relaxation pathways. In these cases, the original nuclear wave packet splits into multiple parts, each dominated by a single electronic state. The average Ehrenfest PES could not represent its individual contributions to the overall relaxation process. AIMC quantifies these cases and replaces the original configuration, corresponding to the original EHR trajectory, by two new configurations. At the cloning event, each new configuration will have the same nuclear wave function but different electronic populations and, therefore, their own distinct mean fields. After that, each new trajectory follows its own mean field PES and separates from the other. More details and technical implementations of the AIMC method can be found elsewhere.[61,86−88]

II.C. Pure Dephasing and Decoherence Time. The correlation between the excited states I and J and the normal modes coupled to the electronic subsystem is usually quantified by the autocorrelation function within the linear response theory:[89]

$$C_{IJ}(t) = \langle \delta E_{IJ}(t) \delta E_{IJ}(0) \rangle \tag{5}$$

where $\delta E_{IJ}(t)$ is the energy gap between states I and J and the angular brackets mean average over all the trajectories. The pure dephasing $D_{IJ}(t)$ is defined by the second order cumulant approximation:[89]

$$D_{IJ}(t) = \exp\left(-\frac{1}{\hbar^2} \int_0^t \mathrm{d}t' \int_0^{t'} \mathrm{d}t'' \, C_{IJ}(t'') \right) \tag{6}$$

Decoherence time τ_{IJ} between electronic states I and J is obtained by fitting the pure dephasing $D_{IJ}(t)$ to a Gaussian function:

$$D_{IJ}(t) \approx \exp\left(-\left(\frac{t}{\tau_{IJ}} \right)^2 \right) \tag{7}$$

II.D. Computational Details. EHR-NEXMD and SH-NEXMD simulations were performed on a halofluorescein dimer (dimer AB, shown in Figure 1a) previously studied

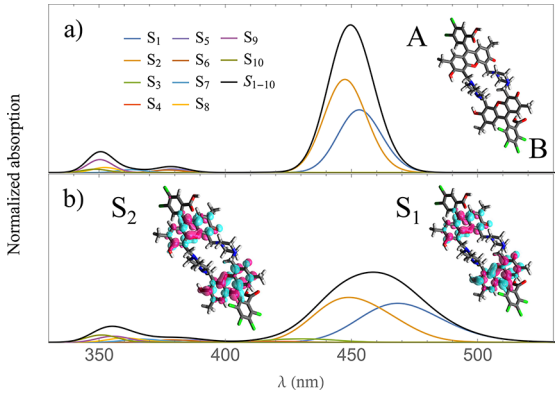

Figure 1. Linear absorption spectra of the AB heterodimer at (a) 10 K and (b) 300 K. Insets in part b show spatial distribution of electronic transition densities of S_1 and S_2 calculated at the ground-state energy minimum.

experimentally using 2D spectroscopy.[29] Both room (300 K) and low (10 K) temperatures were considered. In order to validate the use of EHR method, limited AIMC-MCE-NEXMD simulations were also run for 300 K.

The initial conditions were obtained from an equilibrated ground state molecular dynamics simulation up to 1 ns using Langevin equations with a friction coefficient $\gamma = 2.0\ \text{ps}^{-1}$. The time step for these initial simulations was 0.5 fs. The initial excited states were populated according to a Franck−Condon window given by $g_I(r,R) = f_I \exp[-T^2(E_{laser} - E_I)^2]$ where f_I and E_I are the oscillator strength and energy of excited state I, and E_{laser} is the energy of a Gaussian laser pulse $f(t) = \exp(-t^2/2T^2)$, centered at 450 nm that corresponds to the maximum of the absorption for the S_2 state, with $T^2 = 42.5$ fs corresponding to a fwhm (full width at half-maximum) of 100 fs.

Initial amplitudes $a_I^{(n)}$ for the electronic part of the wave function were set as real values proportional to the square root of $g_I(r,R)$. Nevertheless, tests considering initial random phases have been performed leading to almost indistinguishable average results. The initial value for the current state for SH simulations was chosen randomly according to the initial electronic state populations $|a_I^{(n)}|^2$.

AIMC-MCE simulations were run for 100 initial configurations at 300 K using the same cloning criteria and thresholds as in our previous works.[61,62] We have found that

https://dx.doi.org/10.1021/acs.jpcb.0c01685
J. Phys. Chem. B 2020, 124, 3992−4001

the results given by AIMC-MCE and EHR-MCE calculation are very close for this system. This can be explained by the similarity of the S_1 and S_2 potential energy shapes. As a result, only 13 cloning events happened during these simulations, compared to 383 cloning events per 100 initial conditions in ref.[61] Thus, the bifurcations of the wave function accounted by cloning have minimal effects on the photoinduced energy relaxation of the AB dimer and, in what follows, we restrict our study to results obtained from the direct analysis of the EHR simulations.

Three hundred EHR-NEXMD and SH-NEXMD simulations were run starting from the same set of initial coordinates and velocities. Simulations were performed at constant energy. Six electronic excited states and their corresponding nonadiabatic couplings were included. The time step for EHR and AIMC-MCE simulations was set to 0.05 and 0.1 fs for SH simulations. For AIMC-MCE simulations, Gaussian widths for the nuclear part of the wave function $|\chi_n\rangle$ were taken from the average tested parameters given by Thomson et al.[90] The Min-Cost algorithm has been used to identify and track trivial unavoided crossings, as has been described elsewhere.[64] The instantaneous decoherence approach, where the electronic wave function is collapsed following attempted hop (either successful or forbidden), was introduced to account for electronic decoherence during SH simulations.[91]

III. RESULTS AND DISCUSSION

The photoinduced dynamics of the experimentally studied[19,29] halofluorescein AB heterodimer (Figure 1(a)) at high (300 K) and low (10 K) temperatures has been simulated using SH, EHR and AIMC-MCE approaches (see subsections II.A and II.B). The calculated linear absorption spectra are displayed in Figure 1, where the individual contributions of each state are also shown. These spectra were built as histograms of the excited state energies and oscillator strengths obtained from the set of configurations collected during the equilibrated ground state molecular dynamics simulations at specific temperature. The peak centered near 450 nm at 10 K has dominant contributions from S_1 and S_2 states; it becomes thermally broadened at room temperature due to conformational fluctuations and mixing of excited states. This peak corresponds to the maximum of the previously measured experimental spectra at 524 nm.[29]

The insets in Figure 1b show the spatial localization of the electronic transition density for the S_1 and S_2 states at the minimum of the ground state potential energy surface. One can see equivalent contributions from both monomers due to the coupling between their corresponding excited states. These transition densities identify the lowest excited states as Davydov's pair of Frenkel excitons being symmetric (S_2) and antisymmetric (S_1) combinations of the wave functions of the corresponding monomeric counterparts.

By using these obtained molecular conformations as initial conditions and laser excitation centered at maximum absorption of S_2 state (see subsection II.D), we further perform nonadiabatic dynamics simulations using different methods. Figure 2 shows the calculated time-evolution of populations for S_1 and S_2 states at 10 (a) and 300 K (b).

While both simulations shown in Figure 2 start from different temperature-defined molecular conformation ensembles, they have similar initial conditions of S_2 predominately photoexcited at about 70%. Moreover, after the initial photoexcitation, an ultrafast exchange between both states

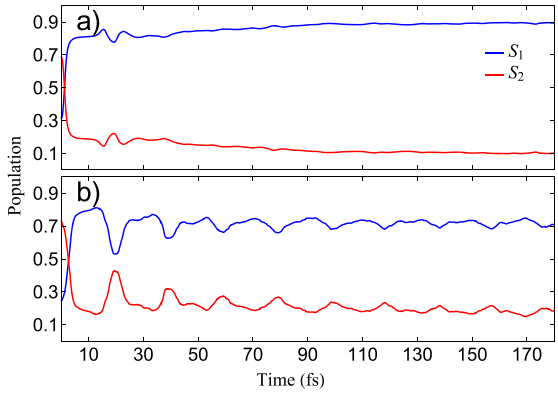

Figure 2. Average populations of S_1 and S_2 electronic states as a function of time at (a) 10 and (b) 300 K obtained using EHR-NEXMD simulations.

takes place during the first ∼5 fs of dynamics. However, the dynamics of populations are distinctly different for 10 and 300 K. At 300 K in Figure 2b, we find persistent quantum beating between both populations lasting up to ∼100 fs with gradual subsequent dephasing. Notably, this is consistent with the oscillating behavior persisting up to ∼100 fs previously experimentally observed by 2D electronic spectroscopy at room temparature.[29]

In contrast, the EHR simulations at 10 K (Figure 2a) does not show any substantial quantum beating that are subdued after the first 40 fs, indirectly suggesting an involvement of thermally induced vibrations in these oscillations. We further stress here that the only difference in simulations at 300 and 10 K is solely in their initial molecular conformations sampled at different temperatures. Ultrafast nonadiabatic dynamics modeling presented was performed at constant energy (see subsection II.D) to avoid any artifacts introduced by a classical Langevin-like thermostat. Furthermore, even in the presence of Langevin thermostat in these simulations, the results do not change substantially. This puzzling difference warrants further investigation and clarification.

The underlying mechanisms responsible for the quantum beatings can be analyzed by evaluating the decoherence time τ_{12} obtained by fitting the pure dephasing function $D_{12}(t)$ (see subsection II.C). We obtained values of τ_{12} = 12 and 6 fs for EHR simulations at 10 and 300 K respectively (see Figure S1). As expected, electronic coherence time scale directly linked to the energy gap $\delta E_{12}(t)$, is larger at 10 K compared to that at 300 K. Nevertheless, this value is significantly smaller compared to the experimentally measured value of 90 fs,[29] obtained by 2D electronic spectroscopy at room temperature. Here we attribute this time scale to a convolution of two distinct aspects in our NEXMD simulations that have not been previously considered: the effect of excited state gradients during the nonequilibrium dynamics after photoexcitation, and the role of nonadiabatic couplings between states. Accounting for both phenomena allowed us to reproduce the quantum beatings persisting up to ∼100 fs, in agreement with 2D spectroscopy results.[29] In order to further understand the origin of this periodic oscillatory behavior of electronic populations, Figure 3a displays the evolution in time of the average energy gap between S_1 and S_2 states, $\delta E_{12}(t)$, during EHR-NEXMD simulations. We can observe that this energy gap oscillates at the same frequency as the electronic populations. According to the Hellmann−Feynman theorem,

https://dx.doi.org/10.1021/acs.jpcb.0c01685
J. Phys. Chem. B 2020, 124, 3992−4001

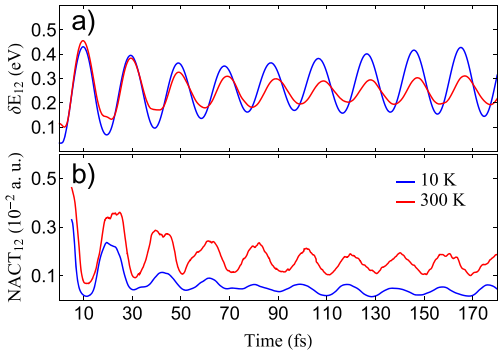

Figure 3. Evolution in time of the (a) average energy gap between S_1 and S_2 states and the (b) average $NACT_{12}$ for EHR-NEXMD simulations.

the nonadiabatic coupling scales as $1/\delta E_{12}(t)$. Therefore, oscillations of $\delta E_{12}(t)$ induce the respective oscillations in the $NACT_{12}$ (see Figure 3b) that is ultimately responsible of the energy transfer between S_1 and S_2 states. That is, the persistence of periodic oscillations of the exciton−vibrational couplings modulates the electronic quantum beating. Moreover, either at low and room temperature, the photoexcitation places the molecular system in regions of the phase space where the S_1 and S_2 electronic states are strongly coupled, leading to the initial ultrafast population exchange observed in Figure 2. After that, the system seems to cross regions of strong coupling in a periodic way during the time of our simulations. This behavior is more pronounced at room temperature than at low temperature, where oscillations are damped after the initial ∼40 fs.

Figure 3a shows that $\delta E_{12}(t)$ decorrelates faster at 300 K than at 10 K. This is in agreement with the corresponding previously reported values of decoherence time τ_{12}. Nevertheless, the more dumped $\delta E_{12}(t)$ oscillations at 300 K are not translated to smaller values of $NACT_{12}$. Actually, the average $NACT_{12}$ values, shown in Figure 3b, present noticeably larger oscillations at 300 K than at 10 K. That is, either at high and low temperature, the molecular system crosses regions of strong nonadiabatic coupling in a periodic manner, reaching higher values at 300 K than 10 K.

Nonadiabatic derivative coupling vector d_{12} (see subsection II.A) represents the direction of the main driving force that nuclei experience while passing regions of phase space with large couplings between states. Figure 4a shows that it corresponds to delocalized nuclei motions, which are equally distributed between both monomers. The similarity of d_{12} among different EHR-NEXMD trajectories has been evaluated performing singular value decomposition (SVD) of matrices $\mathbf{A}(t)$, whose columns are the normalized $d_{12}(t)$ obtained from each EHR-NEXMD trajectory.[92] The overlap between the first SVD vector (SVD_1) and original d_{12} vectors can be considered as a measurement of the similarity of the direction of d_{12} among all the EHR-NEXMD trajectories. Figure 4b shows the evolution in time of the overlap $SVD_1 \cdot d_{12}$ during EHR-NEXMD trajectories at room temperature. A high density of values of $SVD_1 \cdot d_{12} \approx 1$ indicates that all trajectories experience equivalent vibronic couplings, that means equivalent main driving force experienced by nuclei in regions of strong coupling between states. Therefore, Figure 4b shows that, each time the molecular system reaches the region of strong nonadiabatic coupling, the EHR-NEXMD trajectories are

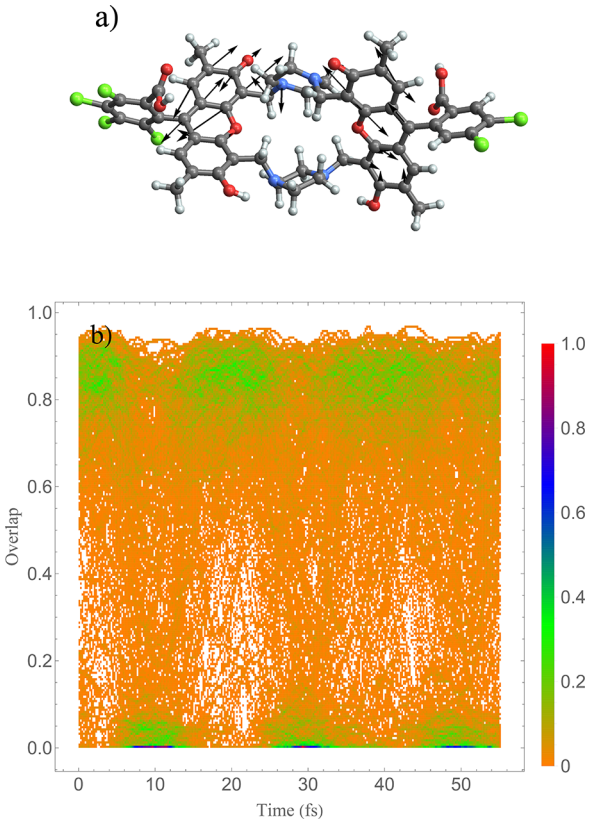

Figure 4. (a) Typical direction of nonadiabatic coupling vector, d_{12}, at ∼20 fs time, when the molecular systems reaches a region of large couplings between S_1 and S_2 states. (b) Density plot of the time evolution of the overlap between the representative SVD_1 vector and d_{12} during EHR-NEXMD trajectories. The bar on the left shows the intensity scale. The color bar corresponds to the number of trajectories at each time.

resynchronized by a common unique driving force in the direction of SVD_1. Since $NACT_{12}$ values are larger at 300 K than 10 K, this effect allows a more effective resynchronization of EHR-NEXMD trajectories at higher temperature, that is translated to the more efficient and cohesive electronic population transfer shown in Figure 2.

As it has been pointed out by numerous previous works using model Hamiltonians,[25,26,35−40] coherent exciton−vibrational dynamics, that emerges from nonadiabatic transitions between excited states, can persists over long time scales at room temperature.[4−7] Nonadiabatic transitions between excited states funnel the energy through specific vibrational motions. Consequently, the nonequilibrium dynamics of such selected vibrations modulates the beating of excitonic populations even at ambient conditions. The projection of $NACR_{12}$ vectors on the basis of equilibrium normal modes (see Figure S2) indicates that the main contributions to the vibronic couplings come through high-frequency vibrations with frequencies within the range of 1620−1890 cm^{-1} (i.e., with corresponding classical periods of 20.6−17.6 fs), that directly relates to oscillation periods in Figures 2 and 3. These modes dominate large amplitude motions compared to other modes (see Figure S3). That is, the photoinduced dynamics activates a bundle of vibrations within the frequency range that corresponds to the quantum beating. This set of modes modulates the electronic degrees of freedom up to ∼100 fs, in a good agreement with the long-lived coherence observed

https://dx.doi.org/10.1021/acs.jpcb.0c01685
J. Phys. Chem. B 2020, 124, 3992−4001

experimentally.[29] That is, a transient synchronization of this bundle of specific high-frequency normal modes controls the periodic energy exchange between monomers.[35] Their larger amplitudes at 300 K than that at 10 K (see Figure S3) allow the molecular system to reach regions of the configurational space with larger couplings between S_1 and S_2 states facilitating nonadiabatic transitions. The rest of the modes remains with an average vibrational energy close to its initial equilibrium value $\approx kT$ = 0.026 eV due to the thermostat effect present in the ground state sampling.

For comparison, the time-evolution of electronic populations was also analyzed with SH-NEXMD simulations either at low and room temperature (see Figure 5). In all cases, the initial ultrafast population exchange observed with EHR-NEXMD simulations is reproduced. Nevertheless, the quantum beating is lacking in SH-NEXMD simulations. The main reason for this can be found in the existence of forbidden or frustrated hops[50] that hinder upward $S_1 \rightarrow S_2$ transitions mostly at ~20 fs after photoexcitation. Frustrated hops take place each time the requirement of conservation of energy during $S_1 \rightarrow S_2$ hops cannot be achieved since the velocity reduction required to compensate the potential energy difference between S_1 and S_2 states is greater than the component of the velocity to be adjusted. In other words, a hop is frustrated if the system does not have enough energy to make the hop. These frustrated hops make nonadiabatic transition an essentially singular event and prevent the quantum beating observed in EHR-NEXMD simulations (see Figure S2).

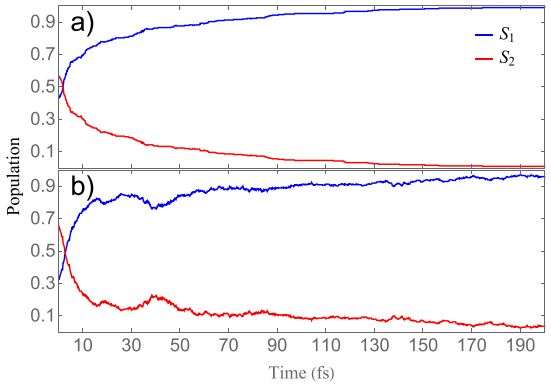

Figure 5. Average populations of S_1 and S_2 electronic states as a function of time obtained using SH method at (a) 10 K and (b) 300 K.

Observed quantum beatings can be also viewed through the spatial transient exciton localization/delocalization using the electronic transition density matrices (TDM).[69] Figure 6 displays two-dimensional plots of the TDM at different times throughout a typical EHR-NEXMD simulation. First, the absence of significant amplitudes in the off-diagonal quadrants, indicating the absence of charge-transfer character between A and B monomers (i.e., positioning of the electron and the hole on different units), validates a picture that a given heterodimer can be well described by the Frenkel exciton model. Initially at t = 0 fs, the wave function is mainly localized on one monomer (in this example monomer A). The comparison of this initial spatial distribution contrasts with the delocalization between both monomers shown in Figure 1b, insets, calculated at the ground-state energy minimum. Therefore, thermal fluctuations at room temperature localize the S_1 and S_2 states to a single monomer. Indeed, the strength of thermal fluctuations (fwhm of the excitation energy distribution ~0.17 eV) does exceed the coupling (see Figure 3b). Immediately after photo-

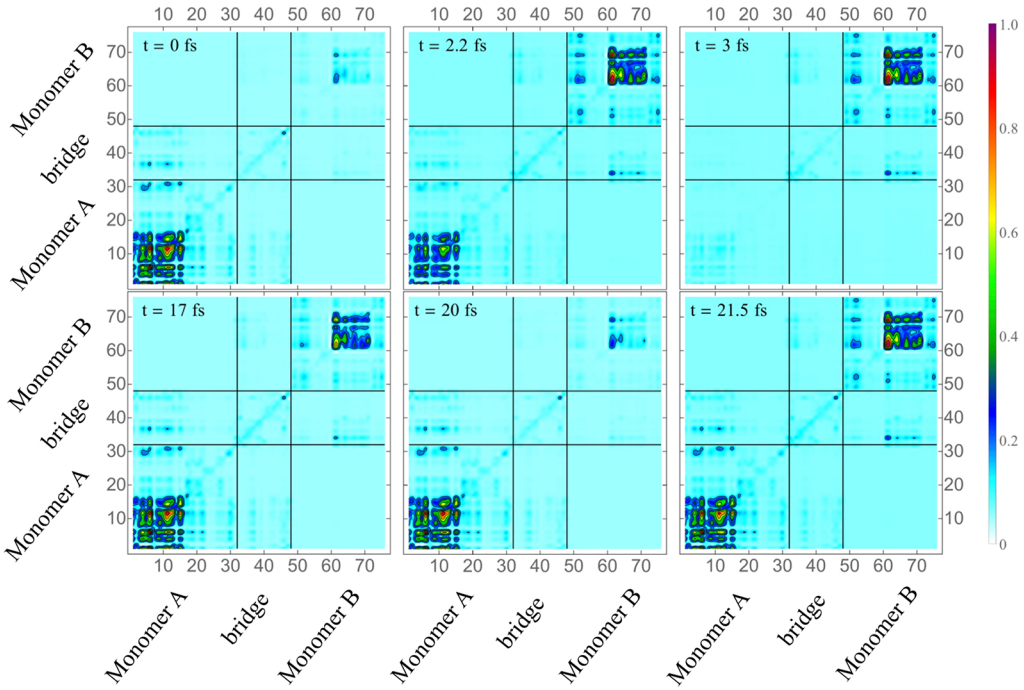

Figure 6. Two-dimensional plots of TDMs for a typical EHR-NEXMD trajectory at 300 K expressed on the basis of atomic orbitals at different times. The x and y axes denote spatial positioning of an electron and a hole in the respective orbitals for atoms ordered along the molecular backbone. The color coding is shown on the side. Block diagonal quadrants correspond to localized excitation on monomer A (lower quadrant) or monomer B (upper quadrant) units, while off-diagonal blocks correspond to charge-transfer contributions.

https://dx.doi.org/10.1021/acs.jpcb.0c01685
J. Phys. Chem. B 2020, 124, 3992−4001

excitation, the AB dimer samples a phase space region of strong coupling between S_1 and S_2 states. This leads to mixing of these states and a transient delocalization of the TDM between both monomers at ∼2.2 fs after photoexcitation. After the first $S_2 \rightarrow S_1$ energy transfer, the TDM becomes transiently localized on monomer B. After ∼17 fs of dynamics, the molecular system experiences a new cross through a strong coupling region (see Figure 3b) and, therefore, the TDM becomes delocalized again. After that, the molecular system passes through the periodic cycles of transient localization and delocalization that are reflected in the quantum beating of the electronic populations shown in Figure 2b.

Finally, Figure 7 shows the time-dependence of the average fraction of electronic transition density localized on each monomer. The average initial transition density localization indicates that it is equally distributed between both monomers (see Figure 7a). This result should not be misinterpreted as a complete exciton delocalization between both monomers. In order to clarify this issue, the average values of fraction of transition density on each monomer have been analyzed separately for trajectories starting mainly localized on each monomer. The results are shown in parts b and c of Figure 7. We can observe that the periodic oscillatory behavior of electronic populations (Figure 2b) induces oscillations in the spatial localization of the electronic transition density between monomers. Thus, the electronic wave function experiences a wave-like spatial localized-delocalized motion during the coherent quantum beating.

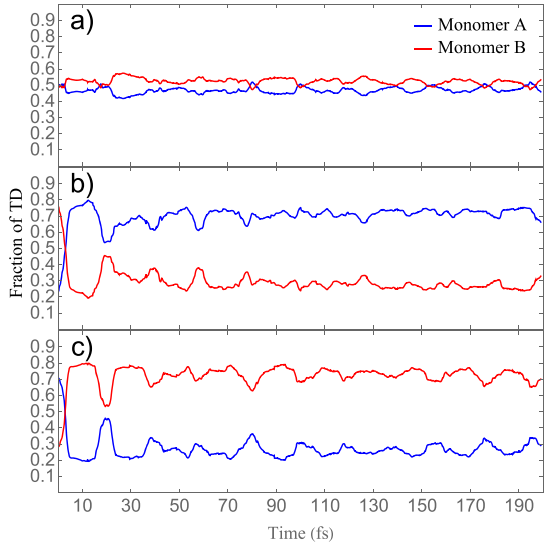

Figure 7. Time-dependence of the fraction of electronic transition density localized on each monomer averaged at 300 K over (a) all the trajectories, (b) those trajectories whose initial transition density is mainly localized on monomer B, and (c) those trajectories whose initial transition density is mainly localized on monomer A.

IV. CONCLUSIONS

The photoexcitation and subsequent electronic and vibrational energy fluxes of a rigid model heterodimer have been analyzed using EHR, SH, and AIMC-MCE methods. We specifically focused on the identification of the mechanisms responsible of the coherent quantum beating of the S_1 and S_2 electronic populations previously reported experimentally reflecting periodic energy transfer between monomers.

After photoexcitation, the EHR simulations at room temperature reveal an ultrafast beating of S_1 and S_2 electronic populations. These oscillations are vibrationally assisted and are not observed at low temperature. Furthermore, they cannot be reproduced by SH method due to multiple forbidden hops.

The observed quantum beating can, in principle, have dual origin. On one hand, the electronic dephasing can be directly related to changes in the energy gaps between states. Our results indicate that this contribution leads to very fast electronic decoherence times that cannot explain the quantum beating. On the other hand, vibronic dynamics can facilitate excited-state coherences. Vibrations at room temperature lead the molecular system to the regions of the configurational space with strong nonadiabatic coupling in a periodic fashion. In turn, this results in the oscillatory population exchanges observed as quantum beating. This is not observed at low temperature, despite the larger electronic and vibrational coherence. At low temperature, nonadiabatic couplings do not feature this periodic behavior and, therefore, periodic population transfer between states quickly vanishes.

Observed persistent nonadiabatic transitions between excited states funnel the energy transfer through specific vibrational motions that modulate the quantum beating between the electronic excited states. Moreover, vibrations whose frequencies are in the range of the electronic population beating are the ones that contribute the most to the direction of the $S_1 \rightarrow S_2$ electronic transitions. That is, the excess of electronic energy flows to vibrations in the presence of strong electron−phonon coupling, creating specific vibrational excitations that ultimately modulate the electronic quantum beating. Consequently, the electronic wave function experiences a wave-like spatial localized-delocalized motion between monomers during the coherent quantum beating.

Overall, our results show that coherent excitonic dynamics is enhanced by the excitation of selected vibrational modes in the direction of the nonadiabatic derivative coupling vector. The efficiency of exciton−vibrational couplings to funnel the energy flux, particularly enhanced at the room temperature, can be associated with its effectiveness to synchronize specific normal mode displacements with oscillations of the excitonic energy splitting. This underpins contributions of vibrational coherences to the long-lived excitonic quantum-beating signals observed in 2D electronic spectra.

Thus, in summary there are two main conclusions of this paper:

1 Ehrenfest method can yield correct dynamics in a situation when surface hopping fails to reproduce the experimentally observed coherent oscillations between electronic states.

2 These oscillations of electronic populations are induced by vibrational motion, and it is essential to take important vibrational modes into account.

■ ASSOCIATED CONTENT

Supporting Information

The Supporting Information is available free of charge at https://pubs.acs.org/doi/10.1021/acs.jpcb.0c01685.

Pure dephasing function, distribution of values of the projection of the SVD1 vector, time evolution of the average kinetic energy, and probability density functions (PDF)

https://dx.doi.org/10.1021/acs.jpcb.0c01685
J. Phys. Chem. B 2020, 124, 3992−4001

AUTHOR INFORMATION

Corresponding Author

S. Fernandez-Alberti − *Departamento de Ciencia y Tecnologia, Universidad Nacional de Quilmes/CONICET, B1876BXD Bernal, Argentina;* orcid.org/0000-0002-0916-5069; Email: sfalberti@gmail.com

Authors

V. M. Freixas − *Departamento de Ciencia y Tecnologia, Universidad Nacional de Quilmes/CONICET, B1876BXD Bernal, Argentina;* orcid.org/0000-0003-1733-4827

S. Tretiak − *Theoretical Division, Center for Nonlinear Studies (CNLS), and Center for Integrated Nanotechnologies (CINT), Los Alamos National Laboratory, Los Alamos, New Mexico 87545, United States;* orcid.org/0000-0001-5547-3647

D. V. Makhov − *School of Chemistry, University of Leeds, Leeds LS2 9JT, U.K.; School of Mathematics, University of Bristol, Bristol BS8 1TW, U.K.*

D. V. Shalashilin − *School of Chemistry, University of Leeds, Leeds LS2 9JT, U.K.;* orcid.org/0000-0001-6104-1277

Complete contact information is available at: https://pubs.acs.org/10.1021/acs.jpcb.0c01685

Notes

The authors declare no competing financial interest.

ACKNOWLEDGMENTS

This work was performed in part at the Center for Nonlinear Studies (CNLS) and the Center for Integrated Nanotechnology (CINT), a U.S. Department of Energy and Office of Basic Energy Sciences user facility. We acknowledge support from the Los Alamos National Laboratory (LANL) Directed Research and Development funds (LDRD). This research used resources provided by the LANL Institutional Computing Program. S.F.-A. and V.M.F acknowledge support of CONICET, UNQ and ANPCyT (PICT-2018-02360). D.V.M. and D.V.S. acknowledge the support from EPSRC through Grant EP/P021123/1.

REFERENCES

(1) Collini, E.; Wong, C. Y.; Wilk, K. E.; Curmi, P. M. G.; Brumer, P.; Scholes, G. D. Coherently Wired Light-Harvesting in Photosynthetic Marine Algae at Ambient Temperature. *Nature* **2010**, *463* (7281), 644−647.

(2) Engel, G. S.; Calhoun, T. R.; Read, E. L.; Ahn, T.-K.; Mančal, T.; Cheng, Y.-C.; Blankenship, R. E.; Fleming, G. R. Evidence for Wavelike Energy Transfer through Quantum Coherence in Photosynthetic Systems. *Nature* **2007**, *446* (7137), 782−786.

(3) Lee, H.; Cheng, Y.-C.; Fleming, G. R. Coherence Dynamics in Photosynthesis: Protein Protection of Excitonic Coherence. *Science* **2007**, *316* (5830), 1462−1465.

(4) Scholes, G. D.; Fleming, G. R.; Chen, L. X.; Aspuru-Guzik, A.; Buchleitner, A.; Coker, D. F.; Engel, G. S.; van Grondelle, R.; Ishizaki, A.; Jonas, D. M.; et al. Using Coherence to Enhance Function in Chemical and Biophysical Systems. *Nature* **2017**, *543* (7647), 647−656.

(5) Mirkovic, T.; Ostroumov, E. E.; Anna, J. M.; van Grondelle, R.; Govindjee; Scholes, G. D. Light Absorption and Energy Transfer in the Antenna Complexes of Photosynthetic Organisms. *Chem. Rev.* **2017**, *117* (2), 249−293.

(6) Brédas, J.-L.; Sargent, E. H.; Scholes, G. D. Photovoltaic Concepts Inspired by Coherence Effects in Photosynthetic Systems. *Nat. Mater.* **2017**, *16* (1), 35−44.

(7) Scholes, G. D.; Fleming, G. R.; Olaya-Castro, A.; van Grondelle, R. Lessons from Nature about Solar Light Harvesting. *Nat. Chem.* **2011**, *3* (10), 763−774.

(8) Kilina, S.; Kilin, D.; Tretiak, S. Light-Driven and Phonon-Assisted Dynamics in Organic and Semiconductor Nanostructures. *Chem. Rev.* **2015**, *115* (12), 5929−5978.

(9) Scholes, G. D. Long-Range Resonance Energy Transfer in Molecular Systems. *Annu. Rev. Phys. Chem.* **2003**, *54* (1), 57−87.

(10) Scholes, G. D.; Rumbles, G. Excitons in Nanoscale Systems. *Nat. Mater.* **2006**, *5* (9), 683−696.

(11) Calhoun, T. R.; Ginsberg, N. S.; Schlau-Cohen, G. S.; Cheng, Y.-C.; Ballottari, M.; Bassi, R.; Fleming, G. R. Quantum Coherence Enabled Determination of the Energy Landscape in Light-Harvesting Complex II. *J. Phys. Chem. B* **2009**, *113* (51), 16291−16295.

(12) Harel, E.; Engel, G. S. Quantum Coherence Spectroscopy Reveals Complex Dynamics in Bacterial Light-Harvesting Complex 2 (LH2). *Proc. Natl. Acad. Sci. U. S. A.* **2012**, *109* (3), 706−711.

(13) Panitchayangkoon, G.; Hayes, D.; Fransted, K. A.; Caram, J. R.; Harel, E.; Wen, J.; Blankenship, R. E.; Engel, G. S. Long-Lived Quantum Coherence in Photosynthetic Complexes at Physiological Temperature. *Proc. Natl. Acad. Sci. U. S. A.* **2010**, *107* (29), 12766−12770.

(14) Hayes, D.; Wen, J.; Panitchayangkoon, G.; Blankenship, R. E.; Engel, G. S. Robustness of Electronic Coherence in the Fenna−Matthews−Olson Complex to Vibronic and Structural Modifications. *Faraday Discuss.* **2011**, *150*, 459.

(15) Christensson, N.; Milota, F.; Hauer, J.; Sperling, J.; Bixner, O.; Nemeth, A.; Kauffmann, H. F. High Frequency Vibrational Modulations in Two-Dimensional Electronic Spectra and Their Resemblance to Electronic Coherence Signatures. *J. Phys. Chem. B* **2011**, *115* (18), 5383−5391.

(16) Tiwari, V.; Peters, W. K.; Jonas, D. M. Electronic Resonance with Anticorrelated Pigment Vibrations Drives Photosynthetic Energy Transfer Outside the Adiabatic Framework. *Proc. Natl. Acad. Sci. U. S. A.* **2013**, *110* (4), 1203−1208.

(17) Knapp, E. W. Lineshapes of Molecular Aggregates, Exchange Narrowing and Intersite Correlation. *Chem. Phys.* **1984**, *85* (1), 73−82.

(18) Souaille, M.; Marchi, M. Nuclear Dynamics and Electronic Transition in a Photosynthetic Reaction Center. *J. Am. Chem. Soc.* **1997**, *119* (17), 3948−3958.

(19) Akimov, A. V.; Prezhdo, O. V. Persistent Electronic Coherence Despite Rapid Loss of Electron−Nuclear Correlation. *J. Phys. Chem. Lett.* **2013**, *4* (22), 3857−3864.

(20) Pachón, L. A.; Brumer, P. Physical Basis for Long-Lived Electronic Coherence in Photosynthetic Light-Harvesting Systems. *J. Phys. Chem. Lett.* **2011**, *2* (21), 2728−2732.

(21) Christensson, N.; Kauffmann, H. F.; Pullerits, T.; Mančal, T. Origin of Long-Lived Coherences in Light-Harvesting Complexes. *J. Phys. Chem. B* **2012**, *116* (25), 7449−7454.

(22) Balevičius, V.; Gelzinis, A.; Abramavicius, D.; Mančal, T.; Valkunas, L. Excitation Dynamics and Relaxation in a Molecular Heterodimer. *Chem. Phys.* **2012**, *404*, 94−102.

(23) Kim, H. W.; Kelly, A.; Park, J. W.; Rhee, Y. M. All-Atom Semiclassical Dynamics Study of Quantum Coherence in Photosynthetic Fenna−Matthews−Olson Complex. *J. Am. Chem. Soc.* **2012**, *134* (28), 11640−11651.

(24) Shim, S.; Rebentrost, P.; Valleau, S.; Aspuru-Guzik, A. Atomistic Study of the Long-Lived Quantum Coherences in the Fenna-Matthews-Olson Complex. *Biophys. J.* **2012**, *102* (3), 649−660.

(25) Kolli, A.; O'Reilly, E. J.; Scholes, G. D.; Olaya-Castro, A. The Fundamental Role of Quantized Vibrations in Coherent Light Harvesting by Cryptophyte Algae. *J. Chem. Phys.* **2012**, *137* (17), 174109.

(26) O'Reilly, E. J.; Olaya-Castro, A. Non-Classicality of the Molecular Vibrations Assisting Exciton Energy Transfer at Room Temperature. *Nat. Commun.* **2014**, *5* (1), 3012.

(27) Caycedo-Soler, F.; Chin, A. W.; Almeida, J.; Huelga, S. F.; Plenio, M. B. The Nature of the Low Energy Band of the Fenna-

Matthews-Olson Complex: Vibronic Signatures. *J. Chem. Phys.* **2012**, *136* (15), 155102.
(28) Collini, E.; Scholes, G. D. Coherent Intrachain Energy Migration in a Conjugated Polymer at Room Temperature. *Science* **2009**, *323* (5912), 369−373.
(29) Hayes, D.; Griffin, G. B.; Engel, G. S. Engineering Coherence Among Excited States in Synthetic Heterodimer Systems. *Science* **2013**, *340* (6139), 1431−1434.
(30) Gambetta, A.; Manzoni, C.; Menna, E.; Meneghetti, M.; Cerullo, G.; Lanzani, G.; Tretiak, S.; Piryatinski, A.; Saxena, A.; Martin, R. L.; et al. Real-Time Observation of Nonlinear Coherent Phonon Dynamics in Single-Walled Carbon Nanotubes. *Nat. Phys.* **2006**, *2* (8), 515−520.
(31) Aggarwal, A. V.; Thiessen, A.; Idelson, A.; Kalle, D.; Würsch, D.; Stangl, T.; Steiner, F.; Jester, S.-S.; Vogelsang, J.; Höger, S.; et al. Fluctuating Exciton Localization in Giant π-Conjugated Spoked-Wheel Macrocycles. *Nat. Chem.* **2013**, *5* (11), 964−970.
(32) Duan, H.-G.; Prokhorenko, V. I.; Cogdell, R. J.; Ashraf, K.; Stevens, A. L.; Thorwart, M.; Miller, R. J. D. Nature Does Not Rely on Long-Lived Electronic Quantum Coherence for Photosynthetic Energy Transfer. *Proc. Natl. Acad. Sci. U. S. A.* **2017**, *114* (32), 8493−8498.
(33) Nelson, T.; Fernandez-Alberti, S.; Roitberg, A. E.; Tretiak, S. Electronic Delocalization, Vibrational Dynamics, and Energy Transfer in Organic Chromophores. *J. Phys. Chem. Lett.* **2017**, *8* (13), 3020−3031.
(34) Nelson, T. R.; Ondarse-Alvarez, D.; Oldani, N.; Rodriguez-Hernandez, B.; Alfonso-Hernandez, L.; Galindo, J. F.; Kleiman, V. D.; Fernandez-Alberti, S.; Roitberg, A. E.; Tretiak, S. Coherent Exciton-Vibrational Dynamics and Energy Transfer in Conjugated Organics. *Nat. Commun.* **2018**, *9* (1), 2316.
(35) Siwiak-Jaszek, S.; Olaya-Castro, A. Transient Synchronisation and Quantum Coherence in a Bio-Inspired Vibronic Dimer. *Faraday Discuss.* **2019**, *216*, 38−56.
(36) Chen, H.; Wang, X.; Han, C.-M.; Li, H.-R. Phonon-Mediated Excitation Energy Transfer in a Detuned Multi-Sites System. *J. Phys. B: At., Mol. Opt. Phys.* **2019**, *52* (7), 075501.
(37) Juhász, I. B.; Csurgay, Á. I. Impact of Undamped and Damped Intramolecular Vibrations on the Efficiency of Photosynthetic Exciton Energy Transfer. *AIP Adv.* **2018**, *8* (4), 045318.
(38) Stones, R.; Olaya-Castro, A. Vibronic Coupling as a Design Principle to Optimize Photosynthetic Energy Transfer. *Chem.* **2016**, *1* (6), 822−824.
(39) Zhang, Z.; Wang, J. Origin of Long-Lived Quantum Coherence and Excitation Dynamics in Pigment-Protein Complexes. *Sci. Rep.* **2016**, *6* (1), 37629.
(40) Chen, H.-B.; Chiu, P.-Y.; Chen, Y.-N. Vibration-Induced Coherence Enhancement of the Performance of a Biological Quantum Heat Engine. *Phys. Rev. E: Stat. Phys., Plasmas, Fluids, Relat. Interdiscip. Top.* **2016**, *94* (5), 052101.
(41) Worth, G. A.; Robb, M. A.; Lasorne, B. Solving the Time-Dependent Schrodinger Equation for Nuclear Motion in One Step: Direct Dynamics of Non-Adiabatic Systems. *Mol. Phys.* **2008**, *106* (16−18), 2077−2091.
(42) Curchod, B. F. E.; Martínez, T. J. Ab Initio Nonadiabatic Quantum Molecular Dynamics. *Chem. Rev.* **2018**, *118* (7), 3305−3336.
(43) Ben-Nun, M.; Quenneville, J.; Martínez, T. J. Ab Initio Multiple Spawning: Photochemistry from First Principles Quantum Molecular Dynamics. *J. Phys. Chem. A* **2000**, *104* (22), 5161−5175.
(44) Makhov, D. V.; Symonds, C.; Fernandez-Alberti, S.; Shalashilin, D. V. A b Initio Quantum Direct Dynamics Simulations of Ultrafast Photochemistry with Multiconfigurational Ehrenfest Approach. *Chem. Phys.* **2017**, *493*, 200−218.
(45) Richings, G. W.; Polyak, I.; Spinlove, K. E.; Worth, G. A.; Burghardt, I.; Lasorne, B. Quantum Dynamics Simulations Using Gaussian Wavepackets: The VMCG Method. *Int. Rev. Phys. Chem.* **2015**, *34* (2), 269−308.
(46) Ben-Nun, M.; Martínez, T. J. Nonadiabatic Molecular Dynamics: Validation of the Multiple Spawning Method for a Multidimensional Problem. *J. Chem. Phys.* **1998**, *108* (17), 7244−7257.
(47) Nelson, T.; Fernandez-Alberti, S.; Roitberg, A. E.; Tretiak, S. Nonadiabatic Excited-State Molecular Dynamics: Modeling Photophysics in Organic Conjugated Materials. *Acc. Chem. Res.* **2014**, *47* (4), 1155−1164.
(48) Tully, J. C.; Preston, R. K. Trajectory Surface Hopping Approach to Nonadiabatic Molecular Collisions: The Reaction of H + with D 2. *J. Chem. Phys.* **1971**, *55* (2), 562−572.
(49) Tully, J. C. Mixed Quantum-Classical Dynamics. *Faraday Discuss.* **1998**, *110*, 407−419.
(50) Tully, J. C. Molecular Dynamics with Electronic Transitions. *J. Chem. Phys.* **1990**, *93* (2), 1061−1071.
(51) Hammes-Schiffer, S.; Tully, J. C. Proton Transfer in Solution: Molecular Dynamics with Quantum Transitions. *J. Chem. Phys.* **1994**, *101* (6), 4657−4667.
(52) Shalashilin, D. V. Quantum Mechanics with the Basis Set Guided by Ehrenfest Trajectories: Theory and Application to Spin-Boson Model. *J. Chem. Phys.* **2009**, *130* (24), 244101.
(53) Fiedler, S. L.; Eloranta, J. Nonadiabatic Dynamics by Mean-Field and Surface-Hopping Approaches: Energy Conservation Considerations. *Mol. Phys.* **2010**, *108* (11), 1471−1479.
(54) Shalashilin, D. V. Nonadiabatic Dynamics with the Help of Multiconfigurational Ehrenfest Method: Improved Theory and Fully Quantum 24D Simulation of Pyrazine. *J. Chem. Phys.* **2010**, *132* (24), 244111.
(55) Shalashilin, D. V. Multiconfigurational Ehrenfest Approach to Quantum Coherent Dynamics in Large Molecular Systems. *Faraday Discuss.* **2011**, *153*, 105.
(56) Saita, K.; Shalashilin, D. V. On-the-Fly Ab Initio Molecular Dynamics with Multiconfigurational Ehrenfest Method. *J. Chem. Phys.* **2012**, *137* (22), 22A506.
(57) Meyer, H.; Miller, W. H. A Classical Analog for Electronic Degrees of Freedom in Nonadiabatic Collision Processes. *J. Chem. Phys.* **1979**, *70* (7), 3214−3223.
(58) Billing, G. D. On the Use of Ehrenfest's Theorem in Molecular Scattering. *Chem. Phys. Lett.* **1983**, *100* (6), 535−539.
(59) Negele, J. W. The Mean-Field Theory of Nuclear Structure and Dynamics. *Rev. Mod. Phys.* **1982**, *54* (4), 913−1015.
(60) Symonds, C.; Kattirtzi, J. A.; Shalashilin, D. V. The Effect of Sampling Techniques Used in the Multiconfigurational Ehrenfest Method. *J. Chem. Phys.* **2018**, *148* (18), 184113.
(61) Freixas, V. M.; Fernandez-Alberti, S.; Makhov, D. V.; Tretiak, S.; Shalashilin, D. An Ab Initio Multiple Cloning Approach for the Simulation of Photoinduced Dynamics in Conjugated Molecules. *Phys. Chem. Chem. Phys.* **2018**, *20* (26), 17762−17772.
(62) Freixas, V. M.; Ondarse-Alvarez, D.; Tretiak, S.; Makhov, D. V.; Shalashilin, D. V.; Fernandez-Alberti, S. Photoinduced Non-Adiabatic Energy Transfer Pathways in Dendrimer Building Blocks. *J. Chem. Phys.* **2019**, *150* (12), 124301.
(63) Fernandez-Alberti, S.; Makhov, D. V.; Tretiak, S.; Shalashilin, D. V. Non-Adiabatic Excited State Molecular Dynamics of Phenylene Ethynylene Dendrimer Using a Multiconfigurational Ehrenfest Approach. *Phys. Chem. Chem. Phys.* **2016**, *18* (15), 10028−10040.
(64) Fernandez-Alberti, S.; Roitberg, A. E.; Nelson, T.; Tretiak, S. Identification of Unavoided Crossings in Nonadiabatic Photoexcited Dynamics Involving Multiple Electronic States in Polyatomic Conjugated Molecules. *J. Chem. Phys.* **2012**, *137* (1), 014512.
(65) Mukamel, S. Trees to Trap Photons. *Nature* **1997**, *388* (6641), 425−427.
(66) Tretiak, S.; Chernyak, V.; Mukamel, S. Recursive Density-matrix-spectral-moment Algorithm for Molecular Nonlinear Polarizabilities. *J. Chem. Phys.* **1996**, *105* (19), 8914−8928.
(67) Tretiak, S.; Zhang, W. M.; Chernyak, V.; Mukamel, S. Excitonic Couplings and Electronic Coherence in Bridged Naphthalene Dimers. *Proc. Natl. Acad. Sci. U. S. A.* **1999**, *96* (23), 13003−13008.

https://dx.doi.org/10.1021/acs.jpcb.0c01685
J. Phys. Chem. B 2020, 124, 3992−4001

(68) Mukamel, S. Electronic Coherence and Collective Optical Excitations of Conjugated Molecules. *Science* **1997**, *277* (5327), 781−787.
(69) Tretiak, S.; Mukamel, S. Density Matrix Analysis and Simulation of Electronic Excitations in Conjugated and Aggregated Molecules. *Chem. Rev.* **2002**, *102* (9), 3171−3212.
(70) Nelson, T.; Fernandez-Alberti, S.; Chernyak, V.; Roitberg, A. E.; Tretiak, S. Nonadiabatic Excited-State Molecular Dynamics Modeling of Photoinduced Dynamics in Conjugated Molecules. *J. Phys. Chem. B* **2011**, *115* (18), 5402−5414.
(71) Chernyak, V.; Schulz, M. F.; Mukamel, S.; Tretiak, S.; Tsiper, E. V. Krylov-Space Algorithms for Time-Dependent Hartree−Fock and Density Functional Computations. *J. Chem. Phys.* **2000**, *113* (1), 36−43.
(72) Tretiak, S.; Isborn, C. M.; Niklasson, A. M. N.; Challacombe, M. Representation Independent Algorithms for Molecular Response Calculations in Time-Dependent Self-Consistent Field Theories. *J. Chem. Phys.* **2009**, *130* (5), 054111.
(73) Furche, F.; Ahlrichs, R. Adiabatic Time-Dependent Density Functional Methods for Excited State Properties. *J. Chem. Phys.* **2002**, *117* (16), 7433−7447.
(74) Tretiak, S.; Chernyak, V. Resonant Nonlinear Polarizabilities in the Time-Dependent Density Functional Theory. *J. Chem. Phys.* **2003**, *119* (17), 8809−8823.
(75) Tommasini, M.; Chernyak, V.; Mukamel, S. Electronic Density-Matrix Algorithm for Nonadiabatic Couplings in Molecular Dynamics Simulations. *Int. J. Quantum Chem.* **2001**, *85* (4−5), 225−238.
(76) Chernyak, V.; Mukamel, S. Density-Matrix Representation of Nonadiabatic Couplings in Time-Dependent Density Functional (TDDFT) Theories. *J. Chem. Phys.* **2000**, *112* (8), 3572−3579.
(77) Send, R.; Furche, F. First-Order Nonadiabatic Couplings from Time-Dependent Hybrid Density Functional Response Theory: Consistent Formalism, Implementation, and Performance. *J. Chem. Phys.* **2010**, *132* (4), 044107.
(78) Dewar, M. J. S.; Zoebisch, E. G.; Healy, E. F.; Stewart, J. J. P. Development and Use of Quantum Mechanical Molecular Models. 76. AM1: A New General Purpose Quantum Mechanical Molecular Model. *J. Am. Chem. Soc.* **1985**, *107* (13), 3902−3909.
(79) Zheng, F.; Fernandez-Alberti, S.; Tretiak, S.; Zhao, Y. Photoinduced Intra- and Intermolecular Energy Transfer in Chlorophyll a Dimer. *J. Phys. Chem. B* **2017**, *121* (21), 5331−5339.
(80) Alfonso Hernandez, L.; Nelson, T.; Tretiak, S.; Fernandez-Alberti, S. Photoexcited Energy Transfer in a Weakly Coupled Dimer. *J. Phys. Chem. B* **2015**, *119* (24), 7242−7252.
(81) Nelson, T.; Fernandez-Alberti, S.; Chernyak, V.; Roitberg, A. E.; Tretiak, S. Nonadiabatic Excited-State Molecular Dynamics: Numerical Tests of Convergence and Parameters. *J. Chem. Phys.* **2012**, *136* (5), 054108.
(82) Tretiak, S.; Chernyak, V.; Mukamel, S. Two-Dimensional Real-Space Analysis of Optical Excitations in Acceptor-Substituted Carotenoids. *J. Am. Chem. Soc.* **1997**, *119* (47), 11408−11419.
(83) Tretiak, S.; Chernyak, V.; Mukamel, S. Collective Electronic Oscillators for Nonlinear Optical Response of Conjugated Molecules. *Chem. Phys. Lett.* **1996**, *259* (1−2), 55−61.
(84) Fernandez-Alberti, S.; Roitberg, A. E.; Kleiman, V. D.; Nelson, T.; Tretiak, S. Shishiodoshi Unidirectional Energy Transfer Mechanism in Phenylene Ethynylene Dendrimers. *J. Chem. Phys.* **2012**, *137* (22), 22A526.
(85) Shalashilin, D. V.; Child, M. S. The Phase Space CCS Approach to Quantum and Semiclassical Molecular Dynamics for High-Dimensional Systems. *Chem. Phys.* **2004**, *304* (1−2), 103−120.
(86) Makhov, D. V.; Glover, W. J.; Martinez, T. J.; Shalashilin, D. V. Ab Initio Multiple Cloning Algorithm for Quantum Nonadiabatic Molecular Dynamics. *J. Chem. Phys.* **2014**, *141* (5), 054110.
(87) Makhov, D. V.; Saita, K.; Martinez, T. J.; Shalashilin, D. V. Ab Initio Multiple Cloning Simulations of Pyrrole Photodissociation: TKER Spectra and Velocity Map Imaging. *Phys. Chem. Chem. Phys.* **2015**, *17* (5), 3316−3325.
(88) Makhov, D. V.; Martinez, T. J.; Shalashilin, D. V. Toward Fully Quantum Modelling of Ultrafast Photodissociation Imaging Experiments. Treating Tunnelling in the Ab Initio Multiple Cloning Approach. *Faraday Discuss.* **2016**, *194*, 81−94.
(89) Mukamel, S. *Principles of Nonlinear Optical Spectroscopy*; Oxford University Press:1995
(90) Thompson, A. L.; Punwong, C.; Martínez, T. J. Optimization of Width Parameters for Quantum Dynamics with Frozen Gaussian Basis Sets. *Chem. Phys.* **2010**, *370* (1−3), 70−77.
(91) Nelson, T.; Fernandez-Alberti, S.; Roitberg, A. E.; Tretiak, S. Nonadiabatic Excited-State Molecular Dynamics: Treatment of Electronic Decoherence. *J. Chem. Phys.* **2013**, *138* (22), 224111.
(92) Shenai, P. M.; Fernandez-Alberti, S.; Bricker, W. P.; Tretiak, S.; Zhao, Y. Internal Conversion and Vibrational Energy Redistribution in Chlorophyll A. *J. Phys. Chem. B* **2016**, *120* (1), 49−58.

https://dx.doi.org/10.1021/acs.jpcb.0c01685
J. Phys. Chem. B 2020, 124, 3992−4001